



Cite this: *Mater. Adv.*, 2022, 3, 4649

Received 17th March 2022,  
Accepted 20th April 2022

DOI: 10.1039/d2ma00309k

rsc.li/materials-advances

## Smartphone-based digitized recognition of $\text{As}^{3+}$ along with its effectual mitigation in water using a benzothiazole-functionalized molecular scaffold<sup>†</sup>

Somrita Nag,<sup>ab</sup> Amita Mondal,<sup>ac</sup> Harish Hirani<sup>ad</sup> and Priyabrata Banerjee  <sup>ab</sup>

In this work, an innovative azomethine-functionalized chromogenic and electrochemical chemosensor **ABH** [2-((acridin-9-yl)methylene)-1-(benzo[d]thiazol-2-yl)hydrazine] was explored, which was synthesized via a one-pot synthetic route with the aim of prolific and sequential aqueous-phase detection of  $\text{As}^{3+}$  and  $\text{F}^-$ . The chemosensor exhibited distinct colorimetric transformation from yellow to burgundy upon addition of  $\text{As}^{3+}$ , which upon subsequent addition of  $\text{F}^-$  rejuvenated, suggesting a strategic application for designing three-input logic gate imitative electronic circuits derived from Boolean algebra. Several sophisticated wet chemical experiments, for instance, UV-Vis spectroscopy, ESI-MS, cyclic voltammetry, <sup>1</sup>H-NMR spectroscopy, and FTIR spectroscopy along with theoretical computations substantiated the sensing phenomena. Furthermore, the development of an inexpensive portable arsenic sensor kit (**ASK**) in addition to a RGB-based smartphone-coupled diagnostic sensor station for rapid on-field detection of  $\text{As}^{3+}$  made the chemosensor an exclusive one as a value-added product in our society. Furthermore, the complexation ability of the sensor with toxic  $\text{As}^{3+}$  introduced it as a smart material for the aqueous-phase elimination of  $\text{As}^{3+}$ .

## 1. Introduction

Arsenic ( $\text{As}^{3+}$ ), one of the most abundant minerals in the earth's crust, causes worldwide intimidation to the ecosystem and human health due to its severe toxicological effects. Drinking water with an elevated concentration of  $\text{As}^{3+}$  causes adverse health effects including arsenicosis, black foot disease, hyperkeratosis, fatigue, genotoxic and mutagenic effects and even cancer. As stated by the World Health Organization (WHO) and the US Environmental Protection Agency (USEPA), the acceptable level for  $\text{As}^{3+}$  in drinking water is 10 ppb.<sup>1</sup> According to the reports, 20 countries worldwide suffer from exceeding  $\text{As}^{3+}$  concentration in drinking water.<sup>2</sup> As a consequence, low-level efficacious recognition of  $\text{As}^{3+}$  in water is of considerable

importance in recent times. The conventional  $\text{As}^{3+}$  detection techniques include atomic absorption spectroscopy (AAS), inductively coupled plasma-mass spectrometry (ICP-MS), atomic fluorescence spectrometry (AFS), inductively coupled plasma-atomic emission spectrometry (ICP-AES), graphite furnace-atomic absorption spectrometry (GF-AAS), and hydride generation-atomic absorption spectrometry (HG-AAS), which are highly expensive, time-consuming and require trained person.<sup>3,4</sup> Moreover, the conventional colorimetric methods for  $\text{As}^{3+}$  recognition, based on the Gutzeit reaction, suffer from fewer optimistic response and lethal by-products such as  $\text{AsH}_3$  gas and mercury compounds.<sup>5a</sup> Therefore, introducing proficient chemical sensors,<sup>5b-d</sup> capable of detecting  $\text{As}^{3+}$  in water is of immense importance to the scientific community. In this perspective, metal nanoparticles have drawn considerable attention over conventional probes, which also suffer from various limitations such as lack of matrix interference, poor stability, high cost and the requirement of special agents to discriminatively detect  $\text{As}^{3+}$ .<sup>6</sup> Conversely, premeditated benzothiazole-functionalized azomethine-based derivatives are acquiring noteworthy consideration owing to their interesting nonlinear optical properties for naked eye detection of  $\text{As}^{3+}$  below the WHO permissible limit.<sup>7</sup>

Therefore, tailor-made synthesis of an inimitable azomethine-functionalized chemosensor, 2-((acridin-9-yl)methylene)-1-(benzo[d]thiazol-2-yl)hydrazine [**ABH**], was explored in this work, which

<sup>a</sup> CSIR-Central Mechanical Engineering Research Institute, M. G. Avenue, Durgapur 713209, India. E-mail: pr\_banerjee@cmeri.res.in, Priyabrata\_banerjee@hotmail.com; Web: <https://www.cmeri.res.in>, <https://www.priyabratabanerjee.in>

<sup>b</sup> Academy of Scientific and Innovative Research (AcSIR), Ghaziabad 201002, Uttar Pradesh, India

<sup>c</sup> Department of Chemistry, National Institute of Technology, M. G. Avenue, Durgapur, 713209, India

<sup>d</sup> Mechanical Engineering Department, Indian Institute of Technology, Delhi-110016, India

<sup>†</sup> Electronic supplementary information (ESI) available. CCDC 2107203. For ESI and crystallographic data in CIF or other electronic format see DOI: <https://doi.org/10.1039/d2ma00309k>



showed unprecedented selectivity and sensitivity towards  $\text{As}^{3+}$  in a water medium. This benzothiazole-functionalized Schiff-base chemosensor was synthesized *via* a one-step condensation reaction by a simple wet chemical method and characterized by several analytical techniques such as ESI-MS, FTIR spectroscopy, SCXRD, and  $^1\text{H}$ -NMR spectroscopy. The presence of aqueous-phase  $\text{As}^{3+}$  can be selectively detected by the rapid colorimetric alteration of the chemosensor from yellow to burgundy even in the presence of other cations, owing to its bis-coordination to the *N,N*-chelate of the benzothiazole derivative, which was further confirmed by  $^1\text{H}$ -NMR titration studies along with density functional theory calculations.<sup>8</sup> Interestingly, the **ABH-As<sup>3+</sup>** adduct was found to be highly efficient to regenerate **ABH** selectively in the presence of  $\text{F}^-$ , one of the most perilous anions due to its various fatal effects such as dental and skeletal fluorosis, and kidney failure in humans,<sup>9</sup> which can further mimic an explicit progression of numerous logical functions, competent of performing molecular-level arithmetic computations.<sup>10</sup> The pH of the ground water  $\text{As}^{3+}$  ranges from pH 5 to pH 6. Consequently, there exists a tendency of interference between the sensing response of  $\text{As}^{3+}$  and sensor solution in acidic pH. After synthesizing the sensor molecule, the halochromic behaviour was investigated. The **ABH** was found to exhibit colorimetric alteration at an extremely lower pH (pH 2), which signified that the sensing response of  $\text{As}^{3+}$  will not interfere with the working pH. Furthermore, to examine any interference caused by the solvatochromic alteration of **ABH** and sensing response of **ABH** with  $\text{As}^{3+}$ , different solvatochromic responses (nonpolar to polar) have been considered and a subtle red-shift in the UV-Vis spectra with the increase in solvent polarity was found. However, in MeOH, like a low-polar protic solvent, compared to highly polar DMSO, such type of chromogenic alteration was not observed. Moreover, MeOH has been selected as sensing media for the high solubility of the sensor. Overall, these solvatochromic and halochromic properties of the sensor strengthen the recognition aptitude of **ABH** towards  $\text{As}^{3+}$ . To the best of our knowledge, this type of sensory probe capable of consecutively detecting both  $\text{As}^{3+}$  and  $\text{F}^-$  is yet to be explored in the literature.

However, updated strategies are required in clinical, food, and environmental realms for rapid analysis using sophisticated instrumentation. In this context, both Analytical Chemistry and Data Management are disciplines of paramount importance. Small, low-cost and portable analytical devices that can be used by inexperienced personnel to acquire accurate and precise data are of significant importance for the betterment of the society.<sup>11</sup> This analytical device should be compatible with resource-limitations such as power supply, laboratory setup and skilled operators. At present, smartphones can be an ideal platform for monitoring contamination in ground water in large areas and the most suitable standpoint for providing device portability, analysis power, data processing and excellent communication abilities. Therefore, in this work, a portable smartphone-based archetype was fabricated in order to have a clear perception about the concentration of  $\text{As}^{3+}$  in groundwater based on the colorimetric alterations of **ABH** in the presence of different concentrations of  $\text{As}^{3+}$ . This Bluetooth-operated smartphone-based prototype will also be

effective to provide contactless data to minimize the risk of direct contact with the contaminants. As per our knowledge, a mobile platform for arsenic detection from ground water with systematized digital response is still less explored in the pertinent research territory.

Moreover, complex-based aqueous-phase mitigation of  $\text{As}^{3+}$  along with its effectual recognition using **ABH** is another advantageous key feature of this probe. Thus, in this work, our prime proposition is based on the exploration of a new economically viable and quick responsive colorimetric chemosensor (**ABH**) for the detection of  $\text{As}^{3+}$  in groundwater with high sensitivity and exceptional selectivity along with a smartphone-based digital response, which was further employed for the sequential recognition of  $\text{F}^-$  and complexation-based mitigation of  $\text{As}^{3+}$ .

## 2. Experimental

### 2.1. Materials

The requisite precursors and other solvents were used without further modification. All the cationic and anionic salts were purchased from Sigma Aldrich and Alfa Aesar Company. Solvents such as acetonitrile, dimethyl sulfoxide, dimethyl formamide, tetrahydrofuran, dichloromethane, hexane, methanol, acetone and water of spectroscopic grade were procured from Merck (India) Pvt. Ltd.

### 2.2. Synthesis and characterization

**ABH** was synthesized *via* a straightforward condensation reaction of 2-hydrazinobenzothiazole and acridine-9-carboxaldehyde in MeOH as a solvent medium along with the catalytic amount of acetic acid (Fig. S1, ESI<sup>†</sup>). The reaction takes place *via* a condensation reaction of aldehyde with a primary amine. After 12 hours of constant stirring, a yellow colored compound was obtained as the sole and end product of the reaction. The product was then collected by solvent evaporation. Yellow colored crystals of **ABH** were obtained by sluggish evaporation of a THF-HXN (1 : 1) solution. **ABH** was thereafter characterized by sophisticated analytical techniques such as CHNS analysis, ESI-MS, HR-MS, FT-IR spectroscopy,  $^1\text{H}$ -NMR spectroscopy (1D and 2D-COSY),  $^{13}\text{C}$ -NMR spectroscopy and UV-Vis spectroscopy to confirm the structure and purity, (*m/z*) calculated 354 for  $\text{C}_{21}\text{H}_{14}\text{N}_4\text{S}$ ; found, 354.8 (**ABH** +  $\text{H}^+$ ) (Fig. S2, ESI<sup>†</sup>). CHN anal. calcd for  $\text{C}_{21}\text{H}_{14}\text{N}_4\text{S}$ : C: 71.16%; H: 3.98%; N: 15.81%; S: 9.05%; found. C: 71.05%; H: 3.13%; N: 15.6%; S: 9%.  $^1\text{H}$ -NMR (400 MHz, solvent: DMSO  $\text{d}^6$ ):  $\delta$  = 9.4 (s, 1H),  $\delta$  = 8.8 (d, 2H,  $J$  = 8.87 Hz),  $\delta$  = 8.2 (d, 2H,  $J$  = 8.21 Hz),  $\delta$  = 7.9 (t, H,  $J$  = 7.92 Hz),  $\delta$  = 7.7 (t, 3H,  $J$  = 7.73),  $\delta$  = 7.5 (d, 2H,  $J$  = 8 Hz),  $\delta$  = 7.35 (t, 1H,  $J$  = 7.36),  $\delta$  = 7.15 (t, 1H,  $J$  = 7.4),  $\delta$  = 6.95 (s, 1H) (Fig. S3a, ESI<sup>†</sup>), 2D COSY  $^1\text{H}$ -NMR (Fig. S3b and Table S9, ESI<sup>†</sup>) and  $^{13}\text{C}$ NMR (Fig. S3c, ESI<sup>†</sup>).

### 2.3. Instrumentation

FT-IR spectroscopy (Spectrum 65, PerkinElmer) was used to confirm the functional groups present within the newly



synthesized **ABH** moiety. The mass of **ABH** was corroborated using a mass spectrometer (Advion Make; Serial no. 3013-0140). A CARY60 spectrophotometer was used to perform the absorbance spectroscopic studies. X-Ray crystallography (Bruker D8 Venture (APEX-III) with photon detector) and <sup>1</sup>H-NMR spectroscopy (Bruker 400 MHz NMR spectrometer) were performed to identify the exact structure and purity of **ABH**. Cyclic voltammetry was carried out using a CH instrument to monitor the electrochemical activity of **ABH**. Atomic absorption spectroscopy (iCE 3500 AAS atomic absorption spectrometer) was accomplished in acquaintance with complex-based  $\text{As}^{3+}$  removal.

#### 2.4. X-Ray crystallographic discussion

The crystals of **ABH** (CCDC No. 2107203) were acquired owing to the sluggish evaporation of the THF-HXN solvent (1:1) mixture (Fig. 1 and Tables S1–S4, ESI<sup>†</sup>). The probe was revealed to be asymmetric in nature. In the thiazole part, the *endo*-cyclic  $-\text{C}=\text{N}$ , C-S bond distance and  $\angle \text{CNC}$  bond angle were found to be 1.29 Å, 1.75 Å and 109.5° respectively, which are almost similar to the conventional benzothiazole moiety with regard to *endo*-cyclic  $-\text{C}=\text{N}$  (1.31 Å), C-S (1.733 Å) bond length and  $\angle \text{CNC}$  (110.62°) bond angle.<sup>12</sup> Moreover, *exo*-cyclic  $-\text{C}=\text{N}$ ,  $-\text{N}-\text{N}$ ,  $-\text{C}=\text{N}$  and C-C bond distances were found to be 1.362 Å, 1.345 Å, 1.29 Å and 1.466 Å respectively. In the acrydine part, the *endo*-cyclic  $-\text{C}=\text{N}$  bond distance and the  $\angle \text{CNC}$  bond angle were found to be 1.35 Å and 118° respectively. Additionally, two **ABH** molecules were interconnected *via* extensive H-bonding interactions between *endo*-cyclic N ( $-\text{C}=\text{N}$ ) and *exo*-cyclic  $-\text{NH}$  groups, which formed a closely packed rectangular dimeric assembly.

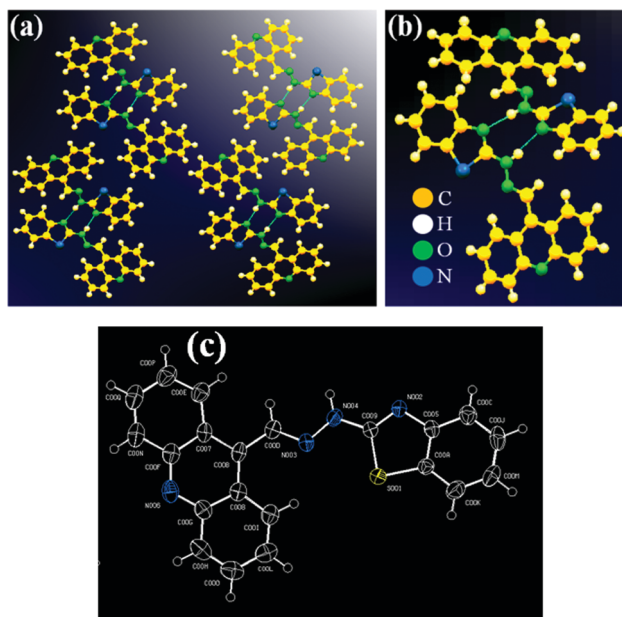


Fig. 1 (a) H-bonding interaction within **ABH** between N of  $-\text{C}=\text{N}$  (ring) and H of  $-\text{NH}$ ; (b) closely packed rectangular shaped structure of **ABH**; and (c) ORTEP image of **ABH** (50% probability).

### 3. Results and discussions

#### 3.1. Solvatochromism and halochromism exhibited by **ABH**

Interesting solvatochromic behavior was noticed for **ABH** in different solvents, wherein bathochromic shifts were observed with the increment in solvent polarity. To confirm these findings, the UV-Vis absorption spectra of **ABH** in both nonpolar and polar solvents (DCM, THF, ACN, MeOH, DMF and DMSO) were investigated [Fig. 2(a)]. The studies revealed that with the increment in solvent polarity from DCM to DMSO, the absorption spectra of **ABH** showed substantial red-shifting from 410 to 430 nm. Basically, enhancement of solvent polarity can stabilize the excited state of molecules and, therefore, diminish the energy gap among ground and excited states, facilitating the charge transfer from the ground state to the excited state at a higher wavelength (*i.e.* lower energy) [Fig. 2(c)].<sup>13,14</sup> In addition, this newly synthesized azomethine-based chemosensor, **ABH**, was professed to specify a particular pH region, establishing the superiority of this chemosensor over previously reported sensory probes. The nature has preserved certain pH-dependent environments to maintain proficient functionalism. Each cell of our body works like a tiny molecular machine and has its own pH-dependent working environment. Alkalinity keeps these tiny machines healthy, whereas an acidic environment spawns an alarm indicating disease.<sup>15–20</sup> In this relevance, the halochromic nature of **ABH** can play a feasible role. The initial base peak of **ABH** appearing at 430 nm remained constant at a biological pH of 6 to 8. However, at pH 2, the peak at 430 nm diminished through the generation of a new peak at 525 nm, indicated by a sharp color change from yellow (color of at biological pH) to violet red, while at pH 4, the peak broadened and **ABH** turned into firebrick color, which could be attributed to the acid-mediated charge transfer within the molecular scaffold. Therefore, these types of pH-dependent colorimetric alterations can further be a footprint towards the development of small molecule-based effectual colorimetric pH sensors [Fig. 2(b and d)].

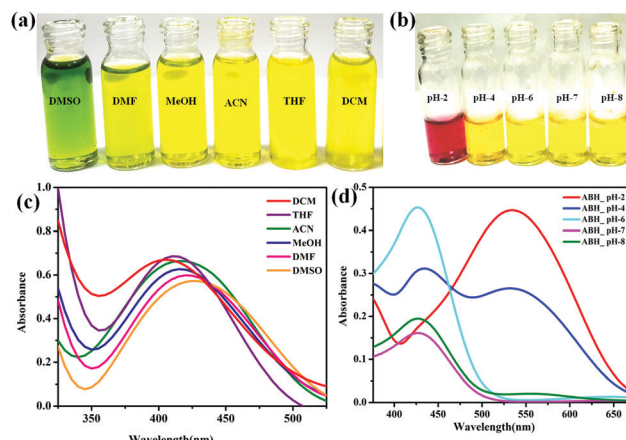


Fig. 2 Pictorial representation of (a) solvatochromism and (b) halochromism exhibited by ( $1 \times 10^{-4}$  M) **ABH**. UV-Vis spectral evidence of (c) solvatochromism and (d) halochromism produced by **ABH**.



### 3.2. Absorbance spectral outcomes of ABH with cations

The chromogenic response of **ABH** in the presence of several analytes is shown in Fig. 3(a), where it can be revealed that the sensor color changed from yellow to burgundy owing to the addition of  $\text{As}^{3+}$ , while it remained unaltered in the presence of other metal ions. The optical response of the probe with  $\text{As}^{3+}$  was validated by UV-Vis spectroscopy. The free sensor showed a peak at 425 nm, which diminished in intensity with the generation of a new peak at 540 nm by the gradual addition of  $\text{As}^{3+}$ , suggesting the charge transfer within the sensor and  $\text{As}^{3+}$  [Fig. 3(b)].<sup>21,22</sup>

The plausible stoichiometric interaction between **ABH** and  $\text{As}^{3+}$  was initially acquainted from Job's plot [Fig. S4, ESI<sup>†</sup>], which revealed the probable binding mode of **ABH** and  $\text{As}^{3+}$  to be 1 : 1. Thenceforward, this possibility of interaction has been well supported by upshot from ESI-MS of **ABH-As<sup>3+</sup>** adducts [Fig. S5, ESI<sup>†</sup>]. The binding constant was also calculated using the Benesi-Hildebrand equation [Table 1 and Fig. S6(a), ESI<sup>†</sup>], which revealed that the binding constant was  $0.47 \times 10^3 \text{ M}^{-1}$ , indicating the effective interaction of the targeted analyte with the sensor moiety. The LOD (limit of detection) was also found to be 5.4 ppb, *i.e.* 72.1 nM [Fig. S6(b), ESI<sup>†</sup>]. Moreover, to get an insight into the requisite time of interaction of **ABH** with  $\text{As}^{3+}$ , the kinetic study was performed, which showed that the mechanistic interaction pathway of **ABH** with  $\text{As}^{3+}$  followed a zero-order reaction kinetics with a rate constant of  $2.6 \times 10^{-3} \text{ mol L}^{-1} \text{ s}^{-1}$ , signifying the independence of rate constant on the concentration of both of the sensor and the analyte [Table 1 and Fig. S7, ESI<sup>†</sup>].<sup>23</sup>

### 3.3. Interference studies of ABH with different cationic analytes

The selectivity of **ABH** towards  $\text{As}^{3+}$  was affirmed from the interference studies, which were conducted by introducing  $\text{As}^{3+}$  into the **ABH** solution containing other competitive cations such as  $\text{Zn}^{2+}$ ,  $\text{Cd}^{2+}$ ,  $\text{Pb}^{2+}$ ,  $\text{Hg}^{2+}$ ,  $\text{Mn}^{2+}$ ,  $\text{Mg}^{2+}$ ,  $\text{Ni}^{2+}$ ,  $\text{Co}^{2+}$ ,  $\text{Cu}^{2+}$ ,  $\text{Fe}^{3+}$ ,  $\text{La}^{3+}$ ,  $\text{Nd}^{3+}$ ,  $\text{Gd}^{3+}$ ,  $\text{Sb}^{3+}$ ,  $\text{Sm}^{3+}$ ,  $\text{Al}^{3+}$ ,  $\text{Cr}^{3+}$ ,  $\text{Au}^{3+}$ ,  $\text{Bi}^{3+}$ , and  $\text{Ca}^{2+}$ .<sup>24</sup> The UV-Vis spectral responses of the **ABH** solution upon addition of  $\text{As}^{3+}$  in the presence of various other cations showed that  $\text{As}^{3+}$  induced an absorbance enhancement at 540 nm, while the other metal ions did not produce any significant variation even if the concentration of interfering ions was much higher than that of  $\text{As}^{3+}$ , indicating high selectivity of **ABH** towards  $\text{As}^{3+}$  [Fig. S8(a-c), ESI<sup>†</sup>]. This excellent selectivity of

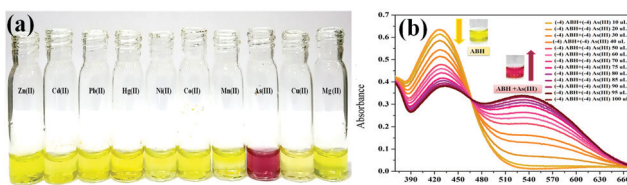


Fig. 3 (a) Visual colorimetric responses of **ABH** ( $1 \times 10^{-4} \text{ M}$ ) in MeOH towards different metal ions ( $1 \times 10^{-4} \text{ M}$ ) in water and (b) UV-Vis absorption spectra of **ABH** ( $10^{-4} \text{ M}$ , MeOH) upon sequential addition of  $\text{As}^{3+}$  ( $10^{-4} \text{ M}$ , water).

Table 1 Interaction of **ABH** with  $\text{As}^{3+}$  in terms of LOD, binding constant and reaction kinetics

Interaction between sensor and incoming analyte	Limit of detection (LOD in ppb)	Binding constant (K in $\text{M}^{-1}$ )	Order and rate of the reaction
<b>ABH-As<sup>3+</sup></b>	5.4 ppb	$0.47 \times 10^3$	$2.6 \times 10^{-3} \text{ mol L}^{-1} \text{ s}^{-1}$

**ABH** towards  $\text{As}^{3+}$  along with its anti-interference potentiality provides a prospective application to make a scrutiny of  $\text{As}^{3+}$  in groundwater.

### 3.4. Real-world application of ABH in determining $\text{As}^{3+}$ in water

The present work was envisaged to detect  $\text{As}^{3+}$  from contaminated ground water samples. Therefore, aliquots of  $300 \mu\text{L}$  of  $\text{As}^{3+}$  of different concentrations (10 ppb, 20 ppb, 50 ppb, 100 ppb and 1 ppm) were added to  $500 \mu\text{L}$  of **ABH** solutions. Immediately, the yellow-colored sensor solution turned into pale yellow, yellowish orange, orange, reddish orange and burgundy as per the incremental concentration of  $\text{As}^{3+}$  [Fig. 4 and Fig. S9(a), ESI<sup>†</sup>]. Hence, **ABH** was perceived to be an efficient chemosensor towards detection of  $\text{As}^{3+}$  in water at both its nontoxic and toxic levels by varying the colorimetric responses, which is of utmost importance in recent times to defeat the worldwide  $\text{As}^{3+}$  contamination.

### 3.5. Development of an $\text{As}^{3+}$ Sensor Kit (ASK) and a Smartphone-coupled diagnostic sensor station for $\text{As}^{3+}$ quantification in water

The concentration-dependent chromogenic sub-micro molar prompt response of **ABH** in the presence of  $\text{As}^{3+}$  instigated us to develop an  $\text{As}^{3+}$  sensor kit (ASK) [Fig. 5(a and b)] and a smartphone-coupled, RGB-based point-of-care testing (POCT) device [Fig. 6(a, b) and Fig. S9(b), ESI<sup>†</sup>] in order to acquire a coherent acuity regarding the concentration of  $\text{As}^{3+}$  in water samples [Fig. S10(a-f), ESI<sup>†</sup>]. Herein, the chemosensor solution ( $0.5 \text{ mL } 10^{-4} \text{ M}$ ) was taken in a vial followed by the addition of  $0.3 \text{ mL}$  contaminated ground water sample. Instantaneous concentration-dependent chromogenic change has been observed upon shaking the vial for 3–5 seconds. The concentration-specific colors of the sensor-analyte solutions were thereafter employed to create a color chart, so that common people can tally the chromogenic change of the sensor after the addition of  $\text{As}^{3+}$  in order to be acquainted with the concentration of  $\text{As}^{3+}$ . Accordingly, a sachet pack of arsenic

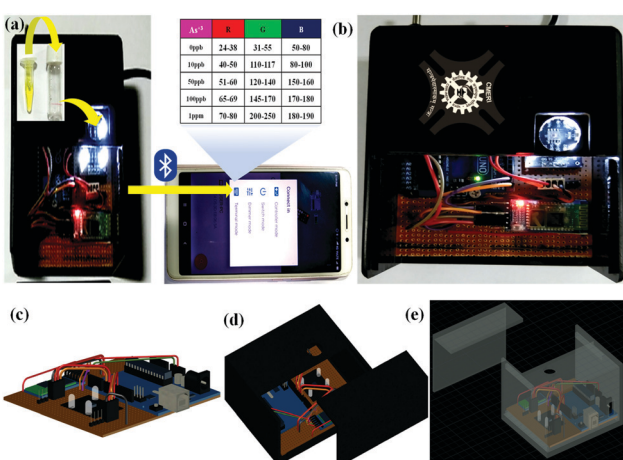


Fig. 4 Pictorial view of the quantitative detection of  $\text{As}^{3+}$  in terms of RGB values.





Fig. 5 (a) Arsenic sensor kit (ASK) and (b) different components of ASK.

Fig. 6 (a) Smartphone-coupled diagnostic sensor station for  $\text{As}^{3+}$  detection; (b) physical image of the fabricated device for the quantitative detection of  $\text{As}^{3+}$ ; (c) 3D CAD model of the circuit of the fabricated device; (d) 3D CAD model of the fabricated device; and (e) X-ray view of the fabricated device.

sensor kit (**ASK**) was developed containing vial 1 (containing a chemosensor solution), vial 2, color chart, working methodology, tissue and soap paper. First, 0.3 mL contaminated water sample will have to be taken within the vial 2 up to the mark. Thereafter, the sensor solution will have to be added from vial 1 to vial 2 to mix the sensor-analyte solution and the observed

color change will have to be tallied with the provided color chart. Therefore, rural people can have a preliminary idea about the concentration of  $\text{As}^{3+}$  in water.

The **ASK** has further been employed towards the development of a Bluetooth-operated portable smartphone-based POCT device depending upon the RGB color code for rapid and on-field recognition of  $\text{As}^{3+}$ . Unambiguously, the fabricated archetype comprises various unique features such as (i) straight measurement of photophysical parameters using integrated sensors, (ii) wireless connectivity with additional devices and (iii) easy operation. The entire prototype is allied with a TCS sensor and a HC-05 Bluetooth SPP module mounted on a designed circuitry board entrenched with a microcontroller along with the boot loader [Fig. S9(b), ESI† and Fig. 6]. The electronic circuitry was positioned in an acrylic-made black box [Fig. 6(b)] to inhibit the infiltration of the surrounding light towards the color sensor. In this device, the concomitant colorimetric responses of **ABH** in the presence of diverse concentrations of  $\text{As}^{3+}$  are recognized by the TCS color sensor and transpired *via* the integrated circuitry and the final output is observed in terms of RGB values on the smartphone *via* Arduino Bluetooth Controller by Giumig Apps. The different RGB values corresponding to different concentrations of  $\text{As}^{3+}$  clearly illustrate the concentration of  $\text{As}^{3+}$  within a specific water solution [Table 2]. Moreover, this Bluetooth-operated module will further take a cutting-edge outline towards the contactless analysis of  $\text{As}^{3+}$ -like toxic analytes for the sustainability of our society. Therefore, this RGB-based Bluetooth-operated smartphone-coupled POCT device can be deployed along with the sachet kit and the table containing the experimentally observed RGB values of different concentration of  $\text{As}^{3+}$  in order to batch scale investigation of  $\text{As}^{3+}$  water samples.

### 3.6. Proposition of electronic circuit fabrication

The attention-grabbing reversible outcomes of **ABH** upon sequential addition of  $\text{As}^{3+}$  and  $\text{F}^-$  [Fig. S12(a and b), ESI†] were employed to design a specific logical circuitry, which imitates a particular sequence of molecular-level arithmetic calculations. Moleculators can perform logical operations based on one or more chemical inputs and a single output. In this case, numerous spectroscopic upshots of the chemical inputs produce a molecular-level complex logic gate circuitry, which can efficiently resolve assorted computational intricacies. The spectroscopic upshots of **ABH** with inward guests,

Table 2 Obtained RGB values in the Smartphone-coupled device after consecutive addition of  $\text{As}^{3+}$  in the sensor

ABH with different concentration of $\text{As}^{3+}$	RGB Range corresponding to the different concentration of $\text{As}^{3+}$ obtained in Smartphone			Color Scale	Safety level after consecutive addition of $\text{As}^{3+}$ in the sensor solution
	R	G	B		
ABH+0ppb $\text{As}^{3+}$	24-38	31-55	50-80		Safe
ABH+10ppb $\text{As}^{3+}$	40-50	110-117	80-100		Moderately safe
ABH+50ppb $\text{As}^{3+}$	51-60	120-140	150-160		Unsafe
ABH+100ppb $\text{As}^{3+}$	65-76	145-170	170-180		Detrimental health impact
ABH+1ppm $\text{As}^{3+}$	78-80	200-250	180-190		Tremendously health threatening

Table 3 Truth table for **ABH** with  $\text{As}^{3+}$  and  $\text{F}^-$ 

Input		Output		
In1 (ABH)	In2 $\text{As}^{3+}$	In3 ( $\text{F}^-$ )	Output Y1 (425 nm)	Output Y2 (525 nm)
0	0	0	0	0
1	0	0	1	0
0	1	0	0	0
0	0	1	0	0
1	1	0	0	1
1	1	1	1	0
0	1	1	0	0
1	0	1	1	0

$\text{As}^{3+}$  and  $\text{F}^-$ , are tabulated in Table 3. Several logic functions such as NAND, NOT, and NOR can be obtained by solving the truth table. A permutation of these logic functions formulates fascinating multifaceted circuits [Fig. 7 and Fig. S11, ESI<sup>†</sup>]. It was evidently observed from the UV-Vis spectra that by the concurrence of  $\text{F}^-$  to the **ABH**- $\text{As}^{3+}$  solution, the peak at 525 nm was omitted with the arrival of the sensor's initial peak at 425 nm, while further addition of  $\text{As}^{3+}$  again produced the response at 525 nm. Therefore, the inputs are as follows: In1: **ABH**; In2:  $\text{As}^{3+}$ ; and In3:  $\text{F}^-$ . In brief, output Y2 will be ON if both inputs 1 (*i.e.*; sensor) and 2 (*i.e.*;  $\text{As}^{3+}$ ) are present. Thus, in the presence of successful input 3 (*i.e.*;  $\text{F}^-$ ) as the inhibitor, it will inhibit the interaction between the sensor and  $\text{As}^{3+}$  by forming  $\text{AsF}_3$ : achievement of the inverter, *i.e.*, NOT gate. Truth Table 2 successfully mimicked the AND-NOT-OR for **ABH**. Hence, the replication of the truth table input along with the output on the suggested logic circuit was accomplished productively.<sup>25,26</sup>

### 3.7. Cyclic voltammetric titration of **ABH** with $\text{As}^{3+}$

The electrochemical experimentation of **ABH** with  $\text{As}^{3+}$  was accomplished in MeOH in an ambience with TBAPF<sub>6</sub> as the supporting electrolyte, which showed noticeable alteration of

the chemosensor's inherent oxidation-reduction potential upon addition of  $\text{As}^{3+}$ . In the absence of  $\text{As}^{3+}$ , the sensor showed quasi-reversibility, while upon addition of  $\text{As}^{3+}$  (120  $\mu\text{L}$ ), the anodic potential at 0.85 V (current height 0.013 mA) and 0.35 V (current height 0.0072 mA) was diminished with the generation of a new peak at 0.52 V (current height 0.0165 mA), indicating the oxidation of the probe upon addition of  $\text{As}^{3+}$ . Additionally, the cathodic potential at 0.7 V (current height 0.0031 mA) and 0.35 V was obtained, signifying the feasibility of the corresponding reduction of the system in the cathode after binding  $\text{As}^{3+}$  [Fig. S13 and Table S5, ESI<sup>†</sup>].

### 3.7. Infrared spectroscopic experimentation of **ABH** with $\text{As}^{3+}$

The infrared spectroscopy of **ABH** was performed in order to have an inclination regarding the host-guest interaction mode. The sensor exhibited a peak at 3408  $\text{cm}^{-1}$ , owing to the N-H stretching vibration of secondary amines and the appearance of a sharp peak at 3074  $\text{cm}^{-1}$  may be attributed to the Ar-CH stretching vibration,<sup>27</sup> while the peaks at 1627  $\text{cm}^{-1}$ , 1557  $\text{cm}^{-1}$  and 750  $\text{cm}^{-1}$  were attributed to the stretching vibration of  $-\text{C}=\text{C}$ ,  $-\text{C}=\text{N}$  and C-S bonds respectively [Fig. S14, ESI<sup>†</sup>]. With the addition of  $\text{As}^{3+}$  to **ABH**, the characteristic peaks in the aromatic region (1450–1650  $\text{cm}^{-1}$ ) were diminished due to interaction with  $\text{As}^{3+}$  via N and S atoms of the probe. Moreover, the reduction of peak intensity in the specific region (1700  $\text{cm}^{-1}$ –1000  $\text{cm}^{-1}$ ) signified the electronic allocation in the host-guest system with the addition of  $\text{As}^{3+}$  [Fig. S15, ESI<sup>†</sup>].<sup>8,28,29</sup>

### 3.8. <sup>1</sup>H-NMR titration of **ABH** with $\text{AsI}_3$

The <sup>1</sup>H-NMR experiments of **ABH** with  $\text{As}^{3+}$  were performed in MeOD and D<sub>2</sub>O solvents with 10<sup>-4</sup> M of the sensor and 10<sup>-4</sup> M targeted analyte solutions in order to affirm the plausible mode of interaction involving **ABH** and  $\text{As}^{3+}$ . The outcome of this study remains in a close-knit with all the spectroscopic and electrochemical experiments [Fig. 8]. With the addition of  $\text{As}^{3+}$ , benzothiazole-functionalized aromatic ring protons ( $\delta$  8.85 ppm and  $\delta$  9.35 ppm) started shifting towards the downfield region, signifying the movement of charge density from **ABH** towards  $\text{As}^{3+}$ , while the decrease in the -NH proton peak signified the interaction between  $\text{As}^{3+}$  with the nearby imine N and benzothiazole ring N centres.<sup>30,31</sup>

### 3.9. Theoretical substantiations

DFT computation was accomplished in the Turbomole (v7.0) in order to expand an obvious perception concerning the plausible mechanistic interaction among **ABH** and  $\text{As}^{3+}$ , which were completely in proportion to the experimental findings. In the case of 1:1 **ABH**:  $\text{As}^{3+}$  adducts, the energies and the HOMO-LUMO gap of the host-guest moiety (1.579 eV) seemed to be inferior than those of the sensor molecule (3.012 eV), suggesting a strong host-guest interaction [Fig. 9]. The interaction energy was evaluated using the following equation:

$$\Delta E_{\text{int}} = E(\text{A}, \text{B}) - [E(\text{A}) + E(\text{B})]$$

where  $E(\text{A}, \text{B})$  is the energy of the **ABH**:  $\text{As}^{3+}$  adduct,  $E(\text{A})$  is the energy of **ABH** and  $E(\text{B})$  is the energy of  $\text{AsI}_3$ . At first, the geometry of **ABH** was optimized having an energy of

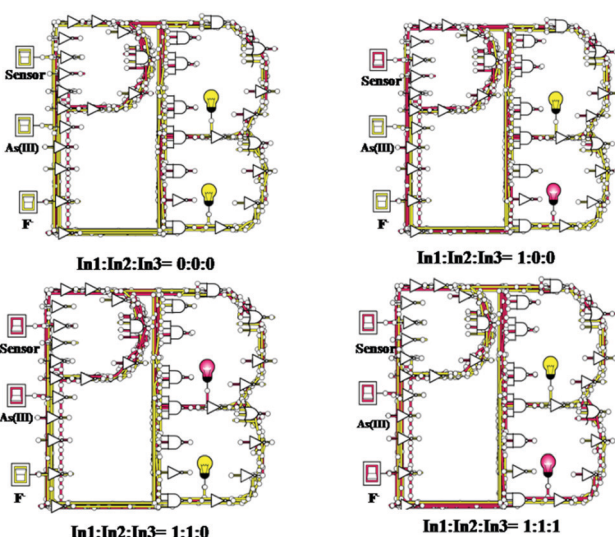


Fig. 7 Fabrication of the three-input logic gate mimic ensemble based on NAND-NOT-NOR logic functions for **ABH** with  $\text{As}^{3+}$  and  $\text{F}^-$ .



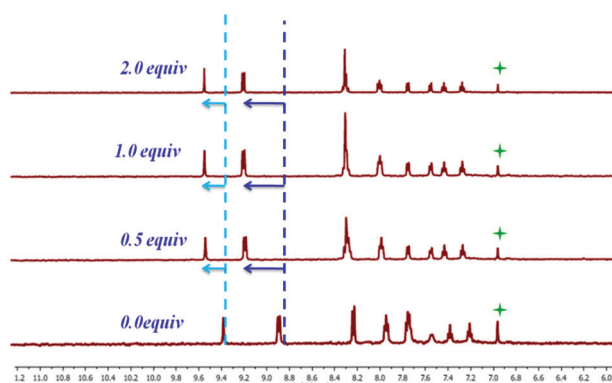


Fig. 8  $^1\text{H}$ -NMR titration of **ABH** with  $\text{As}^{3+}$  (molar ratio of L to  $\text{As}^{3+}$ , 5 : 3) in  $\text{MeOD-D}_2\text{O}$ .

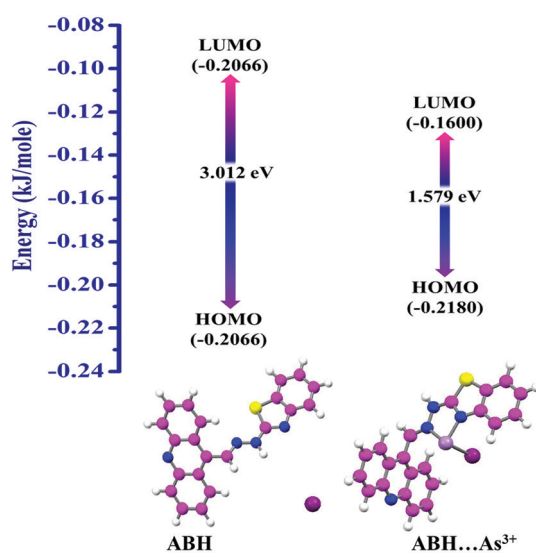


Fig. 9 Geometrically optimized structures of **ABH** with  $\text{As}^{3+}$ .

$-2258.23 \text{ kJ mol}^{-1}$  prior to interaction with  $\text{As}^{3+}$  and the optimized energy of  $\text{AsI}_3$  was found to be  $-2270.07 \text{ kJ mol}^{-1}$ . However, after interaction of **ABH** with  $\text{As}^{3+}$ , the interaction energy ( $\Delta E_{\text{int}}$ ) was found to be  $-1412.62 \text{ kJ mol}^{-1}$ , implying a spontaneous chemical interaction [ESI† and Table 4]. Moreover, the interaction of **ABH** with  $\text{As}^{3+}$  and other interfering lethal trivalent cations was executed. **ABH:As** $^{3+}$  adduct formation was obtained as energetically the most promising among other trivalent cationic adducts with **ABH** [Fig. S16, ESI†], which indicated the selectivity of  $\text{As}^{3+}$  among other trivalent congeners. The Lowdin population analysis in the DFT study reflected that addition of 1 equivalent  $\text{As}^{3+}$  resulted in diminution in electron density on nitrogen atoms of *exo*-cyclic and *endo*-cyclic (benzothiazole part)  $-\text{C}=\text{N}$  units, and the electron density on S atoms of the benzothiazole unit remained slightly rehabilitated, reflecting the feasibility of bis-coordinated *N,N*-chelate formation of the benzothiazole derivative with  $\text{As}^{3+}$ . Furthermore, electron density on the nitrogen

Table 4 Theoretical upshot of **ABH: As** $^{3+}$  interaction

	Total energy ( $\text{kJ mol}^{-1}$ )	HOMO–LUMO gap (eV)	$\Delta E_{\text{int}} = E(\text{A}, \text{B}) - [E(\text{A}) + E(\text{B})]$ ( $\text{kJ mol}^{-1}$ )
<b>ABH</b>	-2837.8307	3.012	—
<b>ABH:As</b> $^{3+}$	-3694.4551	1.579	-1412.62

atom of acrydine part slightly altered due to the drifting of the electron cloud towards arseno-chelate [Table S8, ESI†].

### 3.10. Riddance of $\text{As}^{3+}$ in adulterated water

The complexation capability of **ABH** with  $\text{As}^{3+}$  instigated us to check its mitigation potential of  $\text{As}^{3+}$  in contaminated water. Initially, **ABH** resulted in a colorimetric change from yellow to burgundy upon addition of  $\text{As}^{3+}$  in water, while after a few hours nucleation followed by precipitation was observed at the vial, keeping the upper surface of the solution colorless. The UV-Vis and ESI-MS spectroscopic studies of the complex confirmed the **ABH-As** $^{3+}$  complexation. Therefore,  $\text{As}^{3+}$  ions can be removed by filtering the  $\text{As}^{3+}$  complex from the solution. Furthermore, atomic absorption spectroscopy of the filtrate confirmed that 90% subsidence of  $\text{As}^{3+}$  occurred after separating the **ABH: As** $^{3+}$  adduct [Fig. 10].

### 3.11. Comparative literature survey

In order to explore the advantage of this chemosensor, a thorough literature study was carried out. From the hitherto explored reports, it is observed that most of the probes showed selectivity towards  $\text{As}^{5+}$  and remained silent towards  $\text{As}^{3+}$ , while  $\text{As}^{3+}$  is more toxic than  $\text{As}^{5+}$ . Moreover, some of the synthesized probes showed equal selectivity towards trivalent cations, not specific towards  $\text{As}^{3+}$ . Though plethora of  $\text{As}^{3+}$  detecting probes have been synthesized till date, aqueous-phase detection of  $\text{As}^{3+}$  still can be regarded as a challenge. Ground water contains  $\text{AsO}_2^-$ ,  $\text{AsO}_4^{3-}$ ,  $\text{As}^{3+}$  and  $\text{As}^{5+}$ . Previously, some probes were designed in order to detect  $\text{AsO}_2^-$  (anionic form), which failed to detect  $\text{As}^{3+}$  (cationic form). Somewhere, expensive precursors such as gold salt and environmentally toxic materials were used in order to develop target-specific chemosensors. The newly synthesized chemosensor **ABH** (i) can detect  $\text{As}^{3+}$  from the aqueous phase using a smartphone-coupled device, (ii) can act as an efficient pH sensor by showing halo-chromism and (iii) can detect the solvent purity due to the solvatochromic behavior. Moreover, the newly synthesized chemosensor is

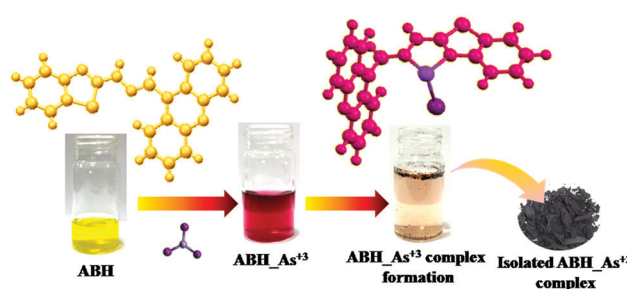


Fig. 10 Removal of  $\text{As}^{3+}$  in water by **ABH**.

nontoxic, inexpensive and shows almost 5 cycles of reversibility with  $\text{F}^-$  [Table S9, ESI†].<sup>31–39</sup>

## Conclusion

Briefly, the newly synthesized inexpensive chemosensor **ABH** can detect highly toxic  $\text{As}^{3+}$  in water with a detection limit (LOD) of 5.4 ppb. The solvatochromic behavior of the newly synthesized chemosensor makes it more efficient to verify the solvent purity, while the halochromism of the probe permits us to treat it as a pH sensor for lower pH values. Furthermore, a logic gate imitating electronic circuitry has been formulated by exploiting the successive reversibility of **ABH** with  $\text{As}^{3+}$  and  $\text{F}^-$ , which further attributes the effective detection efficiency of the probe towards venomous  $\text{As}^{3+}$  and  $\text{F}^-$  reversibly. In addition, the fabricated arsenic sensor kit (**ASK**) and smartphone-coupled diagnostic sensor station introduced the chemosensor as a value-added product in our society, which is explicitly unique of its kind. Moreover, this inimitable probe possesses the integral efficiency towards simultaneous detection and removal of toxic  $\text{As}^{3+}$  as a result of its complexation ability with  $\text{As}^{3+}$ , which made it a smart and efficient material for aqueous-phase elimination of  $\text{As}^{3+}$ .

## Conflicts of interest

There are no conflicts to declare.

## Acknowledgements

The authors sincerely acknowledge DST-DAAD funded project GAP-228512. Authors are thankful to Mr Abhijit Hazra, Research scholar, CSIR-CMERI, for his scientific inputs in designing the sensor molecule. AM is thankful to UGC for her UGC sponsored NFSC fellowship.

## Notes and references

- (a) N. Moghimi, M. Mohapatra and K. T. Leung, Bimetallic Nanoparticles for Arsenic Detection, *Anal. Chem.*, 2015, **87**(11), 5546–5552; (b) A. S. Saleemi, M. Hafeez, A. Munawar, N. Akhtar, W. Abbas, M. E. Mazhar, Z. Shafiq, A. P. Davis and S. L. Lee, Synthesis and Sensing Efficiency of CN Wrapped  $\text{ZnFe}_2\text{O}_4$  Microspheres-Ionic Liquid Composite Towards Ultra-High Sensitivity Arsenic(III) Monitoring of Ground Drinking Water, *J. Mater. Chem. C*, 2020, **8**, 12984–12992; (c) X. Tian, L. Chen, Y. Li,a, C. Yang, Y. Nie, C. Zhoua and Y. Wang, Design and synthesis of molecule with aggregation-induced emission effect and its application in detection of arsenite in groundwater, *J. Mater. Chem. C*, 2017, **5**, 3669–3672.
- C. Gao, X. Y. Yu, S. Q. Xiong, J. H. Liu and X. J. Huang, Electrochemical Detection of Arsenic(III) Completely Free from Noble Metal:  $\text{Fe}_3\text{O}_4$  Microspheres-Room Temperature Ionic Liquid Composite Showing Better Performance than Gold, *Anal. Chem.*, 2013, **85**(5), 2673–2680.
- L. Zhang, X. R. Chen, S. H. Wen, R. P. Liang and J. D. Qiu, Optical sensors for inorganic arsenic detection, *TrAC, Trends Anal. Chem.*, 2019, **118**, 869–879.
- Y. Zhou, X. Huang, C. Liu, R. Zhang, X. Gu, G. Guan, C. Jiang, L. Zhang, S. Du, B. Liu, M. Y. Han and Z. Zhang, Color-Multiplexing-Based Fluorescent Test Paper: Dosage-Sensitive Visualization of Arsenic(III) with Discernable Scale as Low as 5 ppb, *Anal. Chem.*, 2016, **88**(12), 6105–6109.
- (a) L. Zeng, D. Zhou, J. Gong, C. Liu and J. Chen, Highly Sensitive Aptasensor for Trace Arsenic(III) Detection Using DNazyme as the Biocatalytic Amplifier, *J. Anal. Chem.*, 2019, **91**(3), 1724–1727; (b) H. Sharma, N. Kaur, A. Singh, A. Kuwar and N. Singh, Optical Chemosensors for Water Sample Analysis, *J. Mater. Chem. C*, 2016, **4**, 5154–5194; (c) P. Kaur and K. Singh, Recent Advances in Application of BODIPY in Bioimaging and Chemosensing, *J. Mater. Chem. C*, 2019, **7**, 11361–11405; (d) X. N. Qi, L. R. Dang, W. J. Qu, Y. M. Zhang, H. Yao, Q. Lin and T. B. Wei, Based on the phenazine derivatives for optical sensing: a review, *J. Mater. Chem. C*, 2020, **8**, 11308–11339.
- C. I. Weng, J. S. Cang, J. Y. Chang, T. M. Hsiung, B. Unnikrishnan, Y. L. Hung, Y. T. Tseng, Y. J. Li, Y. W. Shen and C. C. Huang, Detection of Arsenic(III) through Pulsed Laser-Induced Desorption/Ionization of Gold Nanoparticles on Cellulose Membranes, *Anal. Chem.*, 2014, **86**(6), 3167–3173.
- (a) S. Lohar, S. Pal, B. Sen, M. Mukherjee, S. Banerjee and P. Chattopadhyay, Selective and Sensitive Turn-on Chemosensor for Arsenite Ion at the ppb Level in Aqueous Media Applicable in Cell Staining, *Anal. Chem.*, 2014, **86**(22), 11357–11361; (b) J. F. Mike, J. J. Inteman, A. Ellern and M. Jeffries-EL, Facile Synthesis of 2,6-Disubstituted Benzobisthiazoles: Functional Monomers for the Design of Organic Semiconductors, *J. Org. Chem.*, 2010, **75**, 495–497; (c) M. Godfroy, J. Liotier, V. M. Mwalukuku, D. Joly, Q. Huaulme, L. Cabau, C. Aumaitre, Y. Kervella, S. Narbey, F. Ostwald, E. Palomares, C. A.-G. Flores, G. Oskam and R. Demadralle, Benzothiadiazole-based photosensitizers for efficient and stable dye-sensitized solar cells and 8.7% efficiency semi-transparent mini-modules, *Sustainable Energy Fuels*, 2021, **5**, 144–153.
- K. Chauhan, P. Singh, B. Kumari and R. K. Singhal, Synthesis of new benzothiazole Schiff base as selective and sensitive colorimetric sensor for arsenic on-site detection at ppb level, *Anal. Methods*, 2017, **9**(11), 1779–1785.
- X. Fan, D. J. Parker and M. D. Smith, Adsorption kinetics of fluoride on low cost materials, *Water Res.*, 2003, **37**(20), 4929–4937.
- A. Mondal, A. Roy Chowdhury, S. Bhuyan, S. K. Mukhopadhyay and P. Banerjee, A simple urea-based multianalyte and multi-channel chemosensor for the selective detection of  $\text{F}^-$ ,  $\text{Hg}^{2+}$  and  $\text{Cu}^{2+}$  in solution and cells and the extraction of  $\text{Hg}^{2+}$  and  $\text{Cu}^{2+}$  from real water sources: a logic gate mimic ensemble, *Dalton Trans.*, 2019, **48**, 4375–4386.
- (a) A. Mukherjee, M. K. Sengupta, M. A. Hossain, S. Ahamed, B. Das, B. Nayak, D. Lodh, M. M. Rahman and D. Chakraborti, Arsenic Contamination in Groundwater: A Global Perspective



with Emphasis on the Asian Scenario, *J. Heal. Popul. Nutr.*, 2006, **24**(2), 142–163; (b) Y. Zhao, M. Gobbi, L. E. Hueso and P. Samori, Molecular Approach to Engineer Two-Dimensional Devices for CMOS and beyond-CMOS Applications, *Chem. Rev.*, 2022, **122**(1), 50–131; (c) S. Franco, J. Garín, N. M.-D. Baroja, R. P. Tejada, J. Orduna, Y. Yu and M. L. Cantu, New D- $\pi$ -A-Conjugated Organic Sensitizers Based on 4H-Pyran-4-ylidene Donors for Highly Efficient Dye-Sensitized Solar Cells, *Org. Lett.*, 2012, **14**(3), 752–755; (d) S. Schumann, R. Da Campo, B. Illy, A. C. Cruickshank, M. A. McLachlan, M. P. Ryan, D. J. Riley, D. W. Mc Comb and T. S. Jones, Inverted organic photovoltaic devices with high efficiency and stability based on metal oxide charge extraction layers, *J. Mater. Chem.*, 2011, **21**, 2381–2386; (e) F. Rosei, M. Schunack, Y. Naitoh, P. Jiang, A. Gourdon, E. Laegsgaard, I. Stensgaard, C. Joachim and F. Besenbacher, Properties of large organic molecules on metal surfaces, *Prog. Surf. Sci.*, 2003, 95–146; (f) M. Chen, L. Lu, H. Yu, C. Li and Ni Zhao, Integration of Colloidal Quantum Dots with Photonic Structures for Optoelectronic and Optical Devices, *Adv. Sci.*, 2021, **8**(18), 2101560.

12 H. G. Raubenheimer, E. K. Marais, S. Cronje, C. Esterhuysen and G. J. Kruger, *J. Chem. Soc., Dalton Trans.*, 2000, 3016–3021.

13 S. Nigam and S. Rutan, Principles and Applications of Solvatochromism, *Appl. Spectrosc.*, 2001, **55**, 362A–370A.

14 A. Marini, A. Muñoz-Losa, A. Biancardi and B. Mennucci, What is solvatochromism?, *J. Phys. Chem. B*, 2010, **114**(51), 17128–17135.

15 S. Halder, S. Dey and P. Roy, A quinoline based Schiff-base compound as pH sensor, *RSC Adv.*, 2015, **5**, 54873–54881.

16 S. Halder, A. Bhattacharjee, A. Roy, S. Chatterjee and P. Roy, Chromogenic and fluorescence sensing of pH with a Schiff-base molecule, *RSC Adv.*, 2016, **6**, 39118–39124.

17 C. Hazneci, K. Ertekin, B. Yenigul and E. Cetinkaya, Optical pH sensor based on spectral response of newly synthesized Schiff bases, *Dyes Pigm.*, 2004, **62**(1), 35–41.

18 K. Jiang, Y. C. Wu, H. Q. Wu, S. L. Li, S. H. Luo and Z. Y. Wang, A highly selective, pH-tolerable and fast-response fluorescent probe for  $Fe^{3+}$  based on star-shape benzothiazole derivative, *J. Photochem. Photobiol. A*, 2018, **350**, 52–58.

19 D. Maity, S. Halder and P. Roy, High pH Sensing Properties of a New Schiff-base Compound, *ChemistrySelect*, 2018, **3**(2), 440–445.

20 V. Kachwal, I. S. Vamsi Krishna, L. Fageria, J. Chaudhary, R. R. Kinkar, R. Chowdhury and I. R. Laskar, Exploring the hidden potential of a benzothiazole-based Schiff-base exhibiting AIE and ESIPT and its activity in pH sensing, intracellular imaging and ultrasensitive & selective detection of aluminium ( $Al^{3+}$ ), *Analyst*, 2018, **143**(15), 3741–3748.

21 V. K. Gupta, A. K. Singh and L. K. Kumawat, Thiazole Schiff base turn-on fluorescent chemosensor for  $Al^{3+}$  ion, *Sens. Actuators, B*, 2014, **195**, 98–108.

22 (a) A. R. Chowdhury, P. Ghosh, S. Paul, S. Bhuyan, J. C.-K. Bose, S. Mukhopadhyay and P. Banerjee, A novel ditopic chemosensor for cadmium and fluoride and its possible application as a pH sensor, *Anal. Methods*, 2017, **9**, 124–133; (b) K. P. Goetz, D. Vermeulen, M. E. Payne, C. Kloc, L. E. McNeilb and O. D. Jurchescu, Charge-transfer complexes: new perspectives on an old class of compounds, *J. Mater. Chem. C*, 2014, **2**, 3065–3076; (c) T. Allen, S. Benis, N. Munera, J. Zhang, S. Dai, T. Li, B. Jia, W. Wang, S. Barlow, D. J. Hagan, E. W. Van Stryland, X. Zhan, J. W. Perry and S. R. Marder, Highly Conjugated, Fused-Ring, Quadrupolar Organic Chromophores with Large Two-Photon Absorption Cross-Sections in the Near-Infrared, *J. Phys. Chem. A*, 2020, **124**(22), 4367–4378.

23 T. R. Knutson, C. M. Knutson, A. R. Mozzetti, A. R. Campos, C. L. Haynes and R. L. Penn, Quantifying Gold Nanoparticle Concentration in a Dietary Supplement Using Smartphone Colorimetry and Google Applications, *J. Chem. Educ.*, 2015, **93**(2), 318–321.

24 A. Mondal, A. Hazra, J. Chakrabarty, K. J.-C. Bose and P. Banerjee, Tandem Detection of Sub-Nano Molar Level  $CN^-$  and  $Hg^{2+}$  in Aqueous Medium by a Suitable Molecular Sensor: A Viable Solution for Detection of  $CN^-$  and Development of the RGB-Based Sensory Device, *ACS Omega*, 2020, **5**(12), 6576–6580.

25 D. Tzeli and I. D. Petsalakis, Physical Insights into Molecular Sensors, Molecular Logic Gates, and Photosensitizers in Photodynamic Therapy, *J. Chem.*, 2019, 6793490.

26 (a) A. R. Chowdhury, P. Ghosh, B. G. Roy, S. K. Mukhopadhyay, P. Mitra and P. Banerjee, A simple and dual responsive efficient new Schiff base chemoreceptor for selective sensing of  $F^-$  and  $Hg^{2+}$ : application to bioimaging in living cells and mimicking of molecular logic gates, *RSC Adv.*, 2015, **5**, 62017–62023; (b) K. M. Poulsen and T. Bjørnholm, Molecular electronics with single molecules in solid-state devices, *Nat. Nanotechnol.*, 2009, **4**, 551–556.

27 M. Sobkowiak and P. Painter, Determination of the aliphatic and aromatic CH contents of coals by FT-ir: studies of coal extracts, *Fuel*, 1992, **71**(10), 1105–1125.

28 S. Erdemir and O. Kocigit, A new perylene bisimide-armed calix [4]-aza-crown as “turn on” fluorescent sensor for  $Hg^{2+}$  ion and its application to living cells, *Sens. Actuators, B*, 2015, **220**, 381–388.

29 S. Daravath, N. Vamsikrishna, N. Ganji, K. Venkateswarlu and Shivaraj, Facile synthesis, structural characterization, DNA binding, incision evaluation, antioxidant and antimicrobial activity studies of Cobalt(II), Nickle(II) and Copper(II) complexes of 3-amino-5-(4-fluorophenyl)isoxazole derivatives, *Chem. Data Collect.*, 2018, **17–18**, 159–168.

30 A. Rambabu, M. Pradeep Kumar, S. Tejaswi, N. Vamsikrishna and Shivaraj, DNA interaction, antimicrobial studies of newly synthesized copper(II) complexes with 2-amino-6-(trifluoromethoxy) benzothiazole Schiff base ligands, *J. Photochem. Photobiol. B*, 2016, **165**, 147–156.

31 A. R. Sadrolhosseini, M. Naseri and H. M. Kamari, Surface plasmon resonance sensor for detecting of arsenic in aqueous solution using polypyrrole-chitosan-cobalt ferrite nanoparticles composite layer, *Opt. Commun.*, 2017, **383**, 132–137.

32 M. Lo Presti, S. El Sayed, R. Martínez-Máñez, A. M. Costero, S. Gil, M. Parra and F. Sancenón, Selective chromo-fluorogenic detection of trivalent cations in aqueous environments using a dehydration reaction, *New J. Chem.*, 2016, **40**, 9042–9045.



33 G. Bhanjana, N. Mehta, G. R. Chaudhary, N. Dilbaghi, K. H. Kim and S. Kumar, Emerging nanobiotechnology in agriculture for the management of pesticide residues, *J. Mol. Liq.*, 2018, **264**, 198–204.

34 A. Bonyár, P. Nagy, V. Mayer, A. Vitéz, A. Gerecs, H. Sántha and G. Harsányi, A colorimetry based, semi-automated portable sensor device for the detection of arsenic in drinking water, *Sens. Actuators, B*, 2017, **251**, 1042–1049.

35 K. Chauhan, P. Singh, B. Kumari and R. K. Singhal, Synthesis of new benzothiazole Schiff base as selective and sensitive colorimetric sensor for arsenic on-site detection at ppb level, *Anal. Methods*, 2017, **9**, 1779–1785.

36 V. C. Ezech and T. C. Harrop, A sensitive and selective fluorescence sensor for the detection of arsenic(III) in organic media, *Inorg. Chem.*, 2012, **51**(3), 1213–1215.

37 J. R. Kalluri, T. Arbneshi, S. A. Khan, A. Neely, P. Candice, B. Varisli, M. Washington, S. McAfee, B. Robinson, S. Banerjee, A. K. Singh, D. Senapati and P. C. Ray, Use of gold nanoparticles in a simple colorimetric and ultrasensitive dynamic light scattering assay: selective detection of arsenic in groundwater, *Angew. Chem., Int. Ed.*, 2009, **48**(51), 9668–9671.

38 J. Li, L. Chen, T. Lou and Y. Wang, Highly Sensitive SERS Detection of As<sup>3+</sup> Ions in Aqueous Media using Glutathione Functionalized Silver Nanoparticles, *ACS Appl. Mater. Interfaces*, 2011, **3**(10), 3936–3941.

39 Y. Wu, S. Zhan, F. Wang, L. He, W. Zhi and P. Zhou, Cationic polymers and aptamers mediated aggregation of gold nanoparticles for the colorimetric detection of arsenic(III) in aqueous solution, *Chem. Commun.*, 2012, **48**, 4459–4461.

